

Machine Learning Sensors for Diagnosis of COVID-19 Disease Using Routine Blood Values for Internet of Things Application

Andrei Velichko ^{1,*}, Mehmet Tahir Huyut ², Maksim Belyaev ¹, Yuriy Izotov ¹ and Dmitry Korzun ¹

¹ Institute of Physics and Technology, Petrozavodsk State University, 33 Lenin str., 185910, Petrozavodsk, Russia

² Department of Biostatistics and Medical Informatics, Faculty of Medicine, Erzincan Binali Yıldırım University, Erzincan, Turkey

* Correspondence: velichko@petrsu.ru (A.V.) tahir.huyut@erzincan.edu.tr (M.T.H);

Abstract: Healthcare digitalization needs effective methods of human sensorics, when various parameters of the human body are instantly monitored in everyday life and connected to the Internet of Things (IoT). In particular, Machine Learning (ML) sensors for the prompt diagnosis of COVID-19 is an important case for IoT application in healthcare and Ambient Assistance Living (AAL). Determining the infected status of COVID-19 with various diagnostic tests and imaging results is costly and time-consuming. The aim of this study is to provide a fast, reliable and economical alternative tool for the diagnosis of COVID-19 based on the Routine Blood Values (RBV) values measured at admission. The dataset of the study consists of a total of 5296 patients with the same number of negative and positive COVID-19 test results and 51 routine blood values. In this study, 13 popular classifier machine learning models and LogNNet neural network model were examined. The most successful classifier model in terms of time and accuracy in the detection of the disease was the Histogram-based Gradient Boosting (HGB). The HGB classifier identified the 11 most important features (LDL, Cholesterol, HDL-C, MCHC, Triglyceride, Amylase, UA, LDH, CK-MB, ALP and MCH) to detect the disease with 100% accuracy, learning time 6.39 sec. In addition, the importance of single, double and triple combinations of these features in the diagnosis of the disease was discussed. We propose to use these 11 traits and their combinations as important biomarkers for ML sensors in diagnosis of the disease, supporting edge computing on Arduino and cloud IoT service.

Keywords: COVID-19; biochemical and hematological biomarkers; routine blood values; feature selection method; LogNNet neural network; Machine Learning sensors, Internet of Medical Things; IoT.

1. Introduction

Identified in 2019, COVID-19 is an infectious disease caused by the novel severe acute respiratory syndrome coronavirus (SARS-CoV-2) [1,2]. Since the World Health Organization (WHO) declared the SARS-CoV-2 infection as a pandemic, the epidemic still maintains its severity [3,4]. In particular, prompt diagnosis of COVID-19 seems a very promising case for applying in at-home healthcare and AAL [5]. Healthcare digitalization needs effective methods of human body sensorics [6], human sensing [7], including ML sensors, when various parameters of the human body are instantly monitored in everyday life and connected to the IoT [8]. This type of everyday human body sensorics has the growing number of applications in IoT-enabled Ambient Intelligence (AmI) systems [9]. The paradigms of ML sensors [10] and Artificial Intelligence (AI) sensoric [11,12] are very similar in meaning. The ML sensor paradigm was further developed by Warden et al. [10] and Matthew Stewart [13], where the authors introduced the terms Sensors 1.0 and Sensors 2.0 devices. Sensors 2.0 devices are a combination of both a physical sensor and a machine learning module in one package. Sensors 2.0 processes data internally, ensuring data security, while in Sensors 1.0 devices these modules are physically separated. In addition, the authors proposed the concept of creating a datasheet of ML sensors. Therefore, the

development of technology for creating ML sensors for the Diagnosis of COVID-19 Disease is an urgent problem.

Many previous studies have indicated that this disease can accompany multi-organ dysfunction and cause a variety of symptoms [3,14–16]. The disease, defined as COVID-19, has been reported to cause severe pneumonia and be associated with severe ARDS, which is thought to be due to an inflammatory cytokine storm [15,17]. The excessive and uncontrolled release of proinflammatory cytokines was considered the most important primary cause of death in coronavirus-related deaths as reported in other infections caused by pathogenic coronaviruses [18].

The pathogen may require special attention in intensive care units (ICUs) and cause a serious respiratory disorder, in some cases leading to death [15,18]. Moreover, it is difficult to distinguish symptoms of COVID-19 from known infections in the majority of patients [15,19,20].

It has been noted in some studies that COVID-19 may be part of a broader spectrum of hyperinflammatory syndromes characterized by cytokine release syndrome (CRS) such as secondary hemophagocytic lymphohistiocytosis (sHLH) [21–23]. Activation of the monocyte-macrophage system just before the disease leads to pneumonia has been reported in previous studies [24,25]. During this period, changes in many routine laboratory parameters such as D-dimer and fibrinogen have been reported in COVID-19 patients [1,2,4,15,17,24,26]. Indeed, it has been reported that high ferritin, D-dimer, lactate dehydrogenase and IL-6 levels are an indicator of poor prognosis and risk of death in patients [27–29]. In addition, Winata and Kurniawan [30] reported increased D-dimer and fibrinogen degradation product (FDP) in all patients in the late stage of COVID-19. This indicates that D-Dimer and FDP levels are elevated due to increased hypoxia in severe COVID-19 conditions and are significantly associated with coagulation. Kurniawan et al. [31] reported that hyperinflammation, coagulation cascade, multi-organ failure, which play a role in the etiopathogenesis of COVID-19, and biomarkers associated with these conditions, such as CRP, D-Dimer, LDH, and albumin, may be useful in predicting the outcome of COVID-19.

Similarly, previous studies have noted the clinical significance of changes in routine blood parameters (RBV) in the prediction of diagnosis and prognosis of infectious diseases [1,2,4,17,32,33]. Despite these clinical features of COVID-19, Jiang et al. [34] and Zheng et al. [35], Huyut and Velichko [36], stated that information on early predictive routine blood parameters, especially for severe and fatal COVID-19 cases, is relatively limited and further studies are needed on larger samples. Similarly, many studies [2,17,37,38] have stated that the relationship between RBVs and the prognosis and severity of COVID-19 should be supported by large datasets.

According to Huyut et al. [15] and Lippi et al. [26] explained that the uncontrolled and rapid spread of diseases during pandemic periods overwhelms health systems, raising concerns about the need for intensive care treatment. In addition, early detection of severely and mildly infected patients in the COVID-19 pandemic is an important and clinically difficult process in terms of morbidity and mortality [15].

Determining whether patients most likely to benefit from supportive care and early intervention are at risk and how to identify them has become the focus of studies [15,39]. However, Banerjee et al. [19] stated that the tests and applications developed for the diagnosis and prognosis of COVID-19 require special equipment and hardware. Without the use of advanced devices and methods, the diagnosis and estimation of the severity of COVID-19 can provide great support to various problems such as patient comfort, health system and economic inadequacies. To this end, Huyut and Üstündağ [38], Huyut and Velichko [36], Beck et al. [40] and Xu et al. [41] reported the development of more economical and faster alternative methods to assist clinical procedures.

The importance of cyberspace in today's era of digitization has changed the way we examine many aspects of life. Many of our goals and future plans are partially or com-

pletely dependent on technology. Therefore, as we are new to this technology-driven environment, we are forced to adopt artificial intelligence (AI) technologies to guide us to improve our processes and adapt to this new culture [42]. Machine learning (ML) and artificial intelligence (AI) approaches provide great convenience in overcoming the difficulties in routine blood values, diagnosis and treatment of COVID-19 patients [36]. Artificial intelligence models are increasingly being used in real-time decision making to reduce drug costs, increase patient comfort, and improve the quality of healthcare services by uncovering hidden relationship structures between features [37,43]. However, it has been stated that if the necessary legal scope and limits for AI applications are not determined, this may lead to negative trends in AI inventions in the future and perhaps have negative effects on national economies [44].

Most of the AI studies used to predict diagnosis, prognosis and mortality of COVID-19 relied on computed tomography (CT) [4,40,43], much less RBVs [37,38,45]. Imaging-based solutions are costly, time consuming and require specialized equipment [45]. Cabitza et al. [45], Huyut and Velichko [36] stated that AI studies based on RBV characteristics can be considered as an effective, rapid and cost-effective alternative for the early detection of the diagnosis and prognosis of COVID-19.

Previous AI studies did not use most RBV parameters and reported relatively lower classifier performance compared to the current study [19,37,38]. Artificial intelligence studies to detect the diagnosis of the disease at an early stage based on RBVs alone are insufficient [38,43,45].

The main theme of ML approaches is the process of transforming the feature vector from the first multidimensional space to the second multidimensional space and determining the vector by a linear classifier [46]. The differences between ML models are usually based on the transformation algorithms and their number and order. Transformation algorithms work by decreasing or increasing the space size. Some popular machine learning classifier algorithms used for data analysis are: multilayer perceptron (feed forward neural network with several layers, linear classifier) [47], support vector machine [48], K-nearest neighbors method [49], XGBoost classifier [50], random forest method [51], logistic regression [52] and decision trees [53].

Since ML algorithms require a sufficiently large number of samples, the dimensionality problem is inevitable in these methods. To minimize this problem, the dataset should be reduced by finding a matrix with fewer columns and similar to the original matrix. Since the new matrix obtained contains fewer features, it is thought that it can be used more efficiently than the original data matrix. Size reduction is the process of obtaining matrices with fewer columns. The dimensionality problem is minimized by discarding irrelevant features with the feature selection procedure [46,54]. In addition, the selection of appropriate features can reduce the measurement cost and provide a better understanding of the hypothesis [46].

Feature selection methods can be summarized under three main headings: embedded methods, filters and wrappers (backward elimination, forward selection, recursive feature elimination) [46,54]. Feature selection in embedded methods is part of the training process and therefore this method lies between filters and wrappers. In embedded methods, the determination of the best subset of features is performed during the training of the classifier (for example, when optimizing weights in a neural network). Therefore, in terms of computational cost, embedded methods are more economical than wrappers [46].

Although we can find many case studies for all three feature selection methods, most feature selection methods are filters [46]. In addition, it can be said that the existence of a large number of available feature selection methods complicates the selection of the best method for a particular problem [54]. Feature selection methods that have become popular recently among researchers are: Correlation-Based Feature Selection (CFS) [55], Consistency-Based Filtering [56], INTERACT [57], Information Gain [58], ReliefF [59], Recursive Feature Elimination for Support Vector Machines (SVM-RFE) [60], Lasso editing [61],

Minimum Redundancy Maximum Relevance (mRMR) algorithm (developed specifically for dealing with microarray data) [46].

In [62], a LogNet neural network-based classifier was described using a handwriting recognition example from the MNIST database. In addition, Velichko [63] demonstrated the use of LogNet to calculate independent risk factors for any disease based on a set of medical health markers. The LogNet neural network passes the feature vector through a special reservoir matrix, transforming it into a feature vector of different size. LogNet can be defined as a direct distribution network that increases the classification accuracy with this function [64]. In a previous study [65], it was noted that a chaotic mapping that fills a reservoir matrix indicates that the increase in entropy value also improves classification accuracy. Accordingly, it is important to optimize the chaotic map parameters in data analysis by applying LogNet neural network. In addition, by taking advantage of chaotic mapping, it is possible to significantly reduce the RAM usage by a neural network. In [63] the algorithm of LogNet operation on a device with 2 kB of RAM is presented. These results showed that LogNet can be used effectively in Internet of Things (IoT) mobile devices.

In this study, we apply 13 classifier machine learning methods and LogNet neural network for the diagnosis of COVID-19 using the RBV values. The latter are measured at the time of admission to the hospital, and identify the most important features in the diagnosis of the disease. We make a clinical interpretation of the relationship between these features and their various combinations with the disease. We also obtain the performance of all models in detecting sick and healthy individuals.

ML sensors (Sensors 1.0 type) for the diagnosis of COVID-19 disease have been successfully tested in the IoT environment, and implements the prognosis of the disease in offline and online modes. In offline mode, ML sensors work on an Arduino board with a LogNet neural network. One of the key conclusion is that this type of human sensorics is expected to move from the very restricted medical lab setting toward the wide market of smart consumer electronics and digital services [9].

The paper has the following structure. Section 2 describes the data collection procedure, correlation analysis of features, machine learning methods, implementing LogNet on an Arduino board. Section 3 presents results on correlation analysis of dataset, classification results, one, double, triple and 11 feature combinations in the detection of sick and healthy individuals, ML sensor concept for IoT. Section 4 discusses the results and compares them with known developments and analysis of results with IoT aspect. In Conclusion, a general description of the study and its scientific significance are given.

2. Materials and Methods

This study was conducted in accordance with the 1989 Declaration of Helsinki. Data were collected retrospectively from the information system of Erzincan Binali Yildirim University Mengücek Gazi Training and Research Hospital (EBYU-MG) between April and December 2021.

In the raw data, RBV data were on a quantitative scale, and diagnostic data were on a multinomial scale. PCR results were filtered from the diagnostic data. Categorical data were coded, repeated measurements were averaged, duplicates were removed, and quantitative data were normalized. Missing RBV data were complemented by the mean of the respective parameter distribution. In the EBYU-MG hospital, only the cases that were detected as SARS-CoV-2 by re-al-time reverse transcriptase polymerase chain reaction (RT-PCR) in nasopharyngeal or oropharyngeal swabs during the dates covered by this study were diagnosed with COVID-19. In order to prevent various complications, RBV results at the first admission were recorded.

2.1. Characteristic of Participants, Workflow and Define Datasets

In this study, we use SARS-CoV-2-RBV1 dataset [36]. Dataset includes the information of 2648 patients diagnosed with COVID-19 and receiving outpatient treatment in hospital on the specified dates, and the same number of patients (control group) whose COVID-19 tests were negative. The control group was randomly selected from individuals over the age of 18 who had applied to the emergency COVID-19 service but had a negative RT-PCR test.

SARS-CoV-2-RBV1 dataset include immunological, hematological and biochemical RBV parameters and consists of 51 features (Table 1). In the SARS-CoV-2-RBV1 dataset, positive COVID-19 test results were coded as 1 and negative as 0 (COVID-19 = 1, non-COVID-19 = 0).

Table 1. Feature numbering for SARS-CoV-2-RBV1 datasets.

No	Feature	No	Feature	No	Feature	No	Feature	No	Feature
1	CRP	12	NEU	23	MPV	34	GGT	45	Sodium
2	D-Dimer	13	PLT	24	PDW	35	Glucose	46	T-Bil
3	Ferritin	14	WBC	25	RBC	36	HDL-C	47	TP
4	Fibrinogen	15	BASO	26	RDW	37	Calcium	48	Triglyceride
5	INR	16	EOS	27	ALT	38	Chlorine	49	eGFR
6	PT	17	HCT	28	AST	39	Cholesterol	50	Urea
7	PCT	18	HGB	29	Albumin	40	Creatinine	51	UA
8	ESR	19	MCH	30	ALP	41	CK		
9	Troponin	20	MCHC	31	Amylase	42	LDH		
10	aPTT	21	MCV	32	CK-MB	43	LDL		
11	LYM	22	MONO	33	D-Bil	44	Potassium		

CRP: C-reactive protein; INR: international normalized ratio; PT: prothrombin time; PCT: Procalcitonin; ESR: erythrocyte sedimentation rate; aPTT: activated partial prothrombin time; LYM: lymphocyte count; NEU: neutrophil count; PLT: platelet count; WBC: white blood cell count; BASO: basophil count; EOS: eosinophil count; HCT: hematocrit; HGB: hemoglobin; MCH: mean corpuscular hemoglobin; MCHC: mean corpuscular hemoglobin concentration; MCV: mean corpuscular volume; MONO: monocyte count; MPV: mean platelet volume; PDW: platelet distribution width; RBC: red blood cells; RDW: red cell distribution width; ALT: alanine aminotransaminase; AST: aspartate aminotransferase; ALP: alkaline phosphatase; CK-MB: creatine kinase myocardial band; D-Bil: direct bilirubin; GGT: gamma-glutamyl transferase; HDL-C: high-density lipoprotein-cholesterol; CK: creatine kinase; LDH: lactate dehydrogenase; LDL: low-density lipoprotein; T-Bil: total bilirubin; TP: total protein; eGFR: estimating glomerular filtration rate; UA: uric acid.

2.2 Correlation analysis of features

To identify a linear relationship between the diagnosis and biochemical blood parameters, the original dataset was analyzed using the Pearson correlation test [66]. For each pair of diagnosis - feature and feature-feature, the Pearson correlation coefficient was calculated and a correlation matrix was compiled. The correlation matrix makes it possible to judge the strength and nature (positive or negative) of the linear relationship between the pairs of diagnosis - feature and feature - feature. The correlation matrix was constructed using the pandas software package [67].

2.3. Machine learning methods, hyperparameters, accuracy estimation

Machine learning algorithms can be applied to a wide range of problems such as classification, clustering, regression analysis, time series forecasting, etc. [68]. The SARS-CoV-2-RBV1 dataset under study has an output parameter divided into two classes (positive or negative diagnosis for COVID-19), so the task of the machine learning algorithm is reduced to binary classification based on 51 features. This study compared the accuracy of the most popular binary classification algorithms:

- Multinomial Naive Bayes (MNB)
- Gaussian Naive Bayes (GNB)
- Bernoulli Naive Bayes (BNB)
- Linear discriminant analysis (LDA)
- K-nearest neighbors (KNN)
- Support vector machine classifier with linear kernel (LSVM)
- Support vector machine classifier with non-linear kernel (NLSVM)
- Passive-aggressive (PA)
- Multilayer perceptron (MLP)
- Decision tree (DT)
- Extra Trees (ET) classifier
- Random forest (RF)
- Histogram based gradient boosting (HGB).

Each classifier model has hyperparameters, the optimization of which is necessary to obtain the most accurate models. For optimization, the software package "auto-sklearn" [69] was used, which is tuned to the target indicator - classification accuracy.

Before training the models, the initial data was subjected to preprocessing, which makes it possible to speed up the training of the models and improve the accuracy of the classification. Preprocessing includes two stages: 1) normalization of numerical values of the input data; 2) generation of additional features. Normalization is a procedure for bringing numerical data to a single format, which has the following options: Quantile transformer (QT) - transforms feature values so that they correspond to a uniform or normal distribution; Robust scaler (RS) - subtracts the median values for each feature and scales according to the interquartile range; MinMax (MM) - scales feature values so that they are all in the range from the minimum to the maximum value. The procedure for generating additional features transforms the original set of features into a set of features with a different dimension. This helps to select the most important features, compose additional features from them, or present the input data in a special format for the ML algorithm. The following methods for generating additional features were used: Polynomial (PN) - creates features that are polynomial combinations of the original features; Random trees embedding (RTE) - creates a multidimensional sparse feature representation, in which the data in each new feature is represented by binary values; Extra trees preprocessor (ETP) - selects a part of the most important features that are evaluated using the Extra trees algorithm; Linear SVM preprocessor (LSVMP) - selects some of the most important features that are evaluated using the Support Vector Machine algorithm; Independent component analysis (ICA) - selects a set of statistically independent features from the entire original set; Nystroem sampler (NS) - transforms a set of initial features using a low-rank matrix approximation by the Nystrom method.

The accuracy of models A_{NF} was assessed by the K-fold cross-validation method ($K = 5$) encapsulated in software packages, where the designation A_{NF} means the classification accuracy when using NF features. The meaning of the K-fold cross-validation method is to split the original dataset into K parts and sequentially train the model, in which one of the K parts of the dataset is used as a test sample, and the rest as a training sample. Then the obtained values of the classification accuracy on the test samples are averaged. The division of the base into parts is performed using stratification. Such an approach makes it possible to reliably estimate the accuracy of models.

In this work, we also used a less common ML algorithm based on the LogNNet neural network. The LogNNet 51:50:20:2 configuration was used, a detailed description of which in relation to SARS-CoV-2-RBV1 is given by Huyut M.T and Velichko A in [36]. The LogNNet architecture is IoT oriented and can run on devices with low computing resources (Section 2.4).

Each algorithm was given the same amount of time (1 hour) to optimize the hyperparameters. A computer with an AMD Ryzen 9 3950X processor and 64 GB DDR-4 RAM was used to train the models.

2.4 Implementing LogNNet on an Arduino board

The Arduino Nano 33 IoT board was chosen as a prototype IoT edge device with limited computing resources. It is based on a 32-bit Microchip ATSAMD21G18 microcontroller with an ARM Cortex-M0+ computing core, a clock frequency of 48 MHz, 256 KB of flash memory and 32 KB of RAM. The neural network LogNNet 51:50:20:2 from [36] was programmed on the Arduino board and tested. Arduino Nano 33 IoT test circuit, LogNNet architecture and board are shown in Figure 1.

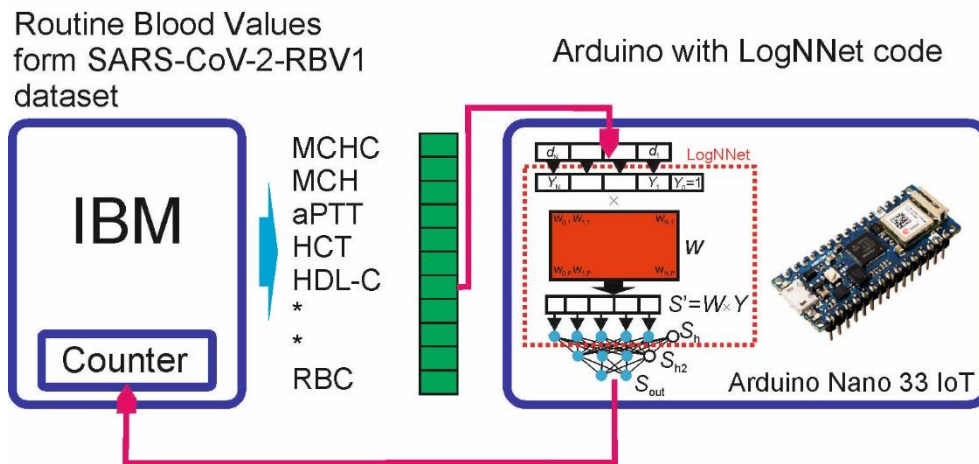


Figure 1. Arduino Nano 33 IoT test circuit and LogNNet architecture.

LogNNet program for Arduino board

The LogNNet principle of operation is to transform the input feature vector d into a normalized vector Y , which is multiplied with the reservoir matrix W filled with a chaotic mapping. In this work, we used the mapping congruent generator (1) with the parameters indicated in Table 2 according to the data of [36]. Then the transformed vector passes the output classifier (two-layer feed-forward neural network with two hidden layers).

Let's denote the matrix of weight coefficients W_1 between the layers S_{h1} - S_{h2} , and W_2 between the layers S_{h2} - S_{out} . At the output, there are 2 neurons for two classes (COVID-19 and non-COVID-19). Matrices of weight coefficients and values of normalization coefficients were calculated on a high performance computer and saved in a separate library file. In addition, the library file (Supplementary Materials) contains the values of K , D , L and C required for calculating the W matrix, and data on configuration of the LogNNet 51:50:20:2 neural network.

Table 2. Chaotic map equation and list of parameters with limits.

Chaotic Map	List of Parameters	Equation
Congruent generator	$K = 93$	$\begin{cases} x_{n+1} = (D - K \cdot x_n) \bmod L \\ x_1 = C \end{cases} \quad (1)$
	$D = 68$	
	$L = 9276$	
	$C = 73$	

When LogNNet is running, the values of the elements of the matrix W (the number of which is 2550) are sequentially calculated using the congruent generator method (1) each time a feature vector is input. This approach allows not to store the matrix W in the RAM memory of the controller, which leads to memory saving, but slows down the calculations of the neural network.

The Arduino IDE development environment was used to implement the algorithm. The library file with the matrices W_1 and W_2 and other coefficients necessary for the operation of the neural network was loaded at the beginning of the program. The complete code of the program is presented in Appendix A, Algorithm A1. The algorithm is divided into functions and procedures:

- Function "Fun_activ" – activation function, lines 10-12;
- Procedure "Reservoir" – calculation of coefficients of reservoir matrix W by congruent generator formula, multiplication of arrays and calculation of neurons in layer S_h , lines 14-28;
- Procedure "Hidden_Layer" – calculation of neurons in the hidden layer S_{h2} , lines 30-39;
- Function "Output_Layer" – calculation of the output layer S_{out} , lines 41-54;
- The "void loop" block is an executable loop, lines 61-77;
- "void setup" block - initialization block, lines 61-77.

The scaling factor "scale_factor = 1000" allows to convert data from a floating point type to an integer (and vice versa), by multiplying (dividing) by a factor and rounding. In the Arduino, a float variable takes up 4 byte RAM, and an integer variable takes up 2 byte RAM. Therefore, storing matrices W_1 , W_2 and other data in integer format is more profitable, and when initializing the library, the data takes up 2 times less RAM memory.

Test scheme

Neural network testing is the serial sending of SARS-CoV-2-RBV1 data to the Arduino board and counting the correct network responses. The data is generated on an external computer (Figure 1). To send data, a protocol was implemented that separates the elements of the feature vector Y using the symbol "T" to avoid data gluing. At the end of the vector Y , special characters "FN" are placed, indicating the end of the data transfer. On the Arduino side, a protocol is implemented that recognizes the input data. In the "void loop" block, a loop is organized to check the availability of data in the serial port buffer using the Serial.available function. This function returns "True" as soon as the Arduino receives data.

3. Results

3.1. Correlation analysis of Dataset SARS-CoV-2-RBV1

Figure 2 shows the results of the correlation analysis of the diagnosis - feature and feature - feature pairs in the form of a “heatmap” over the entire volume of the SARS-CoV-2-RBV1 database. Table 3 shows the features most correlated with the diagnosis, in which the Pearson coefficient exceeds 0.5. For comparison, the results of the threshold classification A_{th} from [36] are presented, features for which $A_{th} \geq 75\%$ are shown. It can be seen that the threshold classification method and the Pearson correlation method give an intersecting set of features, however, the threshold classification gives more features correlated with the diagnosis. This is due to the fact that Pearson’s coefficients well reveal a linear relationship between a feature and a diagnosis, while the diagnosis has only two values (1 and 0), and the threshold method gives better results when separating two classes.

Table 3. Features most strongly correlated with the diagnosis according to the Pearson coefficient and the threshold correlation method.

Feature (Pearson's Coefficient)	Feature (Threshold accuracy of classification A_{th} from [36])
MCHC (0.8)	MCHC (94.35 %)
HDL-C (-0.77)	HDL-C (94.73 %)
Cholesterol (-0.71)	Cholesterol (94.47 %)
LDL (-0.68)	LDL (96.47%)
	Triglyceride (90.96 %)
	Amylase (85.1 %)
	UA (81.12 %)
	TP (79.68 %)
	CK-MB (78.91 %)
	LDH (74.98 %)
	Albumin (72.91 %)

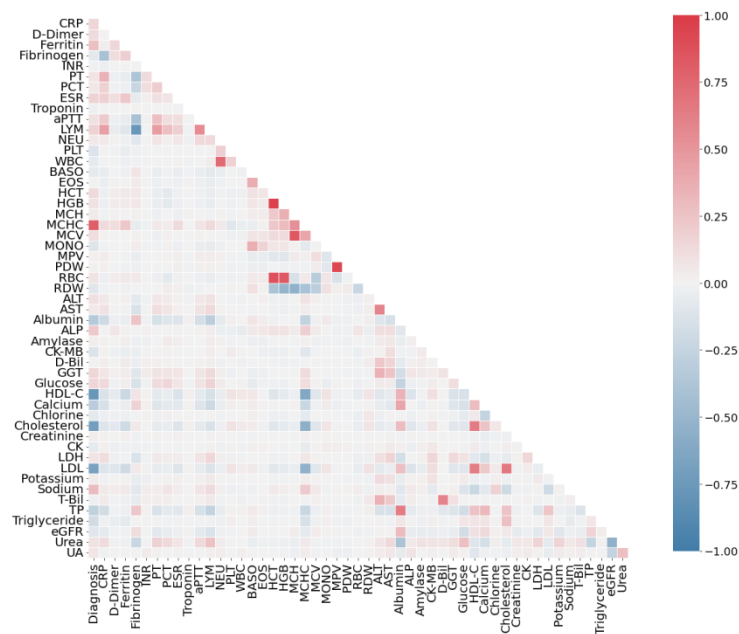


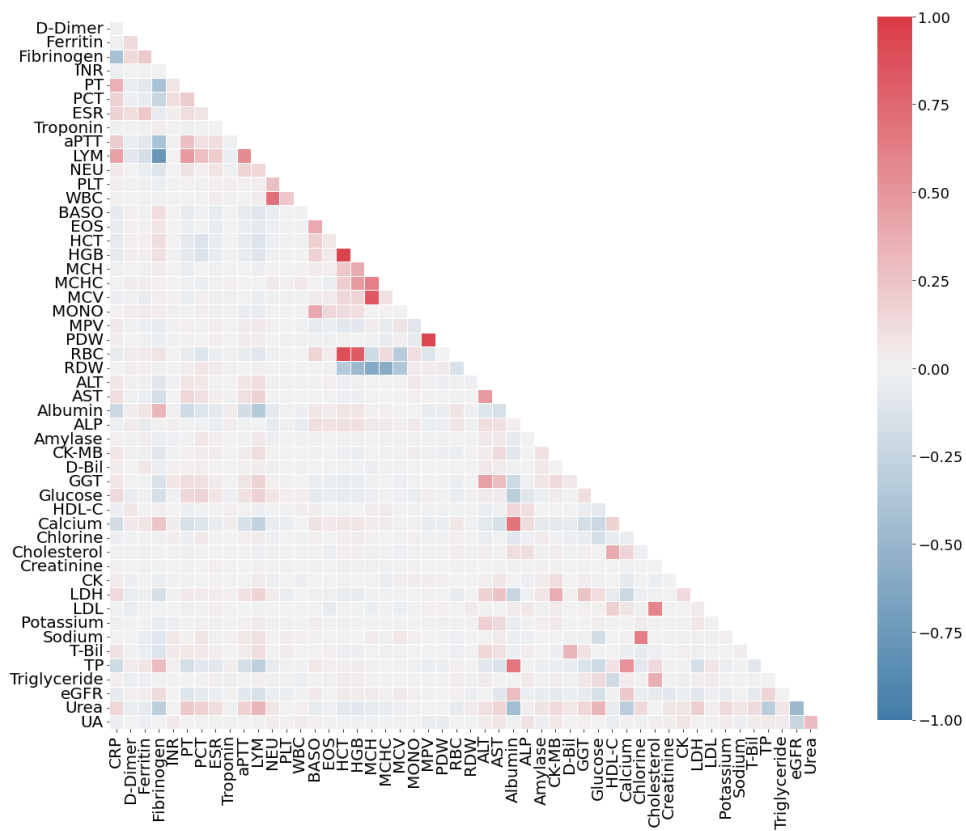
Figure 2. Pearson correlation of the SARS-CoV-2-RBV1 dataset for diagnosis - feature and feature - feature pairs.

An analysis of the correlation of features among themselves (Figure 2) reveals a number of features that are linearly dependent on each other. The most strongly correlated pairs are shown in Table 4 for which the Pearson coefficient exceeds 0.6 modulo. The same table shows Pearson's coefficients separately for a variety of COVID-19 positive and negative participants. Full heatmaps by class (COVID-19, non-COVID-19) are shown in Figure 3.

Table 4. The features most strongly correlated with each other by the Pearson coefficient for the entire database and separately for classes (Positive or Negative COVID-19).

Pair feature- feature	Pearson's coefficient for positive and negative COVID-19	Pearson's coefficient for positive COVID-19	Pearson's coefficient for negative COVID-19
Type High-High			
HCT-HGB	0.96	0.95 (High)	0.97(High)
MPV-PDW	0.93	0.94	0.92
HCT-RBC	0.87	0.88	0.87
MCH-MCV	0.84	0.84	0.84
HGB-RBC	0.83	0.83	0.83
NEU-WBC	0.74	0.71	0.81
Albumin-TP	0.64	0.67	0.5
MCH-MCHC	0.53	0.62	0.99
MCH-RDW	-0.55	-0.61	-0.51
Type High-Low			
Fibrinogen-LYM	-0.77	-0.78 (High)	-0.01 (Low)
Cholesterol-LDL	0.65	0.59	0.012
Cholesterol-HDL-C	0.64	0.39	-0.024
Chlorine-Sodium	0.18	0.63	-0.025
Type Low-High			
MCHC-MCV	0.41	0.09 1(Low)	0.84 (High)
ALT-AST	0.6	0.48	0.76
eGFR-Urea	-0.55	-0.49	-0.63
INR-PT	0.12	0.075	1
D-Bil-T-Bil	0.6	0.33	0.91
HDL-C-LDL	0.63	0.19	0.3

Three main types of pair correlations can be distinguished, (High-High type) these are pairs of features, the correlation of which has a high value, and it does not depend on the presence or absence of COVID-19 disease. There are pairs of features that are highly correlated only in sick patients (High-Low type), or only in healthy patients (Low-High type). Figure 3 also shows that, in general, the features are more correlated in patients with COVID-19. From a medical point of view, pair correlation will be considered in the Discussion section.



(a)

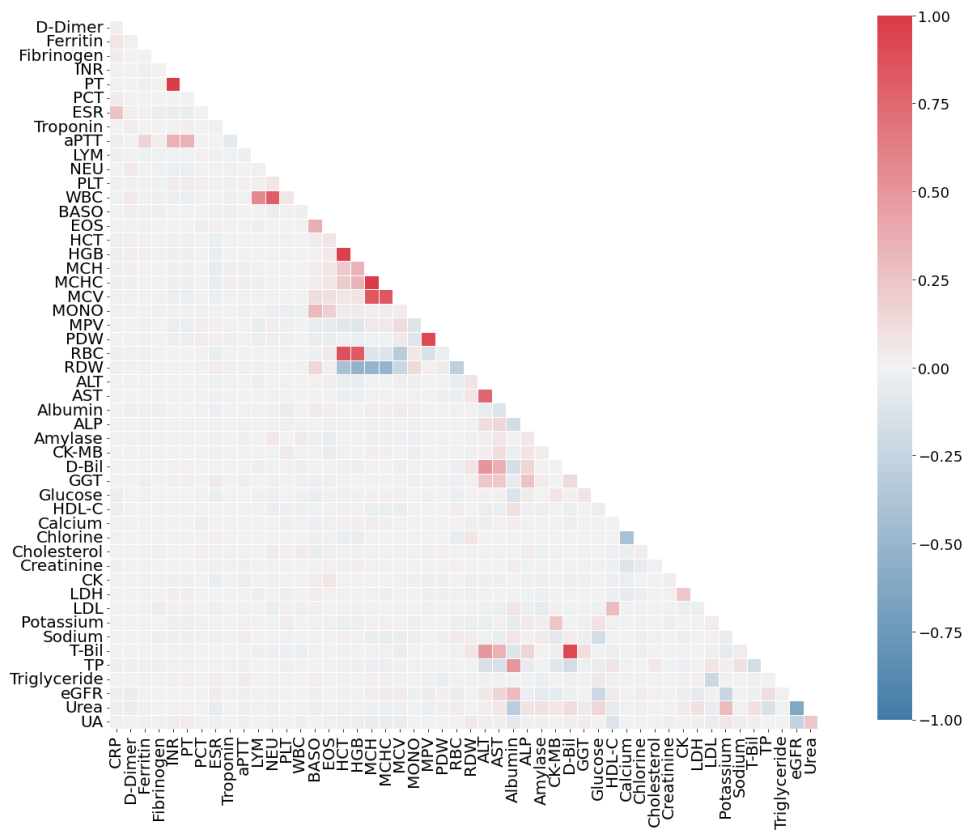


Figure 3. Correlation analysis results for positive (a) and negative (b) diagnoses for COVID-19 from the SARS-CoV-2-RBV1 dataset.

3.2 Classification results for Dataset SARS-CoV-2-RBV1

Table 5 presents the results of the machine learning algorithms optimized to obtain the maximum classification value using 51 features. The results are sorted in descending order of algorithm efficiency. For each algorithm, the average training time of the model in and methods for preprocessing the input data are given.

Table 5. Results of assessing the classification accuracy of machine learning models for the SARS-CoV-2-RBV1 dataset.

Classification algorithm	Average model accuracy A_{51} , %	Average learning time, s	Normalization method	Methods for generating additional features
Histogram based Gradient Boosting	100	6.39	-	-
Random Forest	99.943	13.15	QT	-
K-nearest neighbors	99.924	3.17	QT	ETP
Extra Trees classifier	99.905	18.73	RS	-
Multilayer Perceptron	99.886	3.99	RS	LSVMP
Multinomial Naive Bayes	99.792	2.48	QT	RTE
Linear Discriminant Analysis	99.773	9.15	QT	PN
Support Vector Machine with non-linear kernel	99.754	222.41	QT	NS
Decision Tree	99.660	1.46	RS	LSVMP
Passive-Aggressive	99.641	2.91	QT	RTE
Bernoulli Naive Bayes	99.622	2.59	QT	RTE
Support Vector Machine with linear kernel	99.584	5.21	MM	PN
Gaussian Naive Bayes	98.565	1.68	QT	ICA
LogNNNet [36]	99.509	100	-	-

The accuracy of the algorithms A_{51} ranged from 98.56% to 100%, indicating that all models were good at identifying the association of features with the diagnosis of COVID-19. The most efficient model is based on the Histogram based Gradient Boosting classifier with 100% accuracy. Unlike other models, HGB does not require data preprocessing. The training time of the HGB model is about 6 seconds, which makes it possible to effectively use it to enumerate input features when searching for optimal combinations. The LogNNNet model was used to implement the classification on the Arduino board, so its algorithm has a compact form suitable for IoT devices.

The HGB model was used to study the most significant combinations of the features. Investigation of the effectiveness of the HGB model operating on the 1 feature

Table 6 presents the classification result of SARS-CoV-2-RBV1 datasets for the HGB model using a single input feature. Features are sorted in descending order of A_1 classification accuracy. The most effective features are the first six: LDL (№43), Cholesterol (№39), HDL-C (№36), MCHC (№20), Triglyceride (№48), Amylase (№31). The same features are dominant in assessing the correlation between the sign and the diagnosis from Table 3.

Table 6. Classification efficiency of SARS-CoV-2-RBV1 datasets using the single feature for the Histogram based Gradient Boosting classifier.

Nº	Feature	A ₁ , %	Nº	Feature	A ₁ , %	Nº	Feature	A ₁ , %	Nº	Feature	A ₁ , %
43	LDL	96.84	4	Fibrinogen	76.03	50	Urea	68.10	21	MCV	56.43
39	Cholesterol	95.07	29	Albumin	75.3	7	PCT	63.25	22	MONO	56.26
36	HDL-C	94.99	44	Potassium	75.22	27	ALT	62.33	5	INR	56.19
20	MCHC	94.35	3	Ferritin	74.45	35	Glucose	62.17	6	PT	56.04
48	Triglyceride	93.76	38	Chlorine	73.18	49	eGFR	62.04	17	HCT	55.75
31	Amylase	90.01	46	T-Bil	72.77	14	WBC	61.91	26	RDW	55.62
51	UA	87.91	34	GGT	72.62	16	EOS	61.40	9	Troponin	54.07
42	LDH	85.76	41	CK	70.97	13	PLT	61.25	18	HGB	53.94
47	TP	80.41	2	D-Dimer	70.46	28	AST	60.55	25	RBC	53.43
37	Calcium	80.40	33	D-Bil	70.37	8	ESR	59.12	23	MPV	53.13
32	CK-MB	79.73	11	LYM	69.90	15	BASO	58.72	24	PDW	53.09
1	CRP	77.81	45	Sodium	69.35	12	NEU	57.51	19	MCH	52.13
30	ALP	77.71	40	Creatinine	69.24	10	aPTT	56.53			

Investigation of the effectiveness of the HGB model operating on the 2 features

Table 7 presents the classification result of SARS-CoV-2-RBV1 datasets for the HGB model using two input features. Pairs of features are sorted in descending order of classification accuracy A_2 .

Table 7. Classification efficiency of SARS-CoV-2-RBV1 datasets using 2 features for the Histogram based Gradient Boosting classifier.

Nº	First feature	Second feature	Average accuracy A ₂ , %
20-19	MCHC	MCH	99.81
43-32	LDL	CK-MB	99.62
36-32	HDL-C	CK-MB	99.49
48-32	Triglyceride	CK-MB	99.45
43-39	LDL	Cholesterol	99.43
43-20	LDL	MCHC	99.22
39-36	Cholesterol	HDL-C	99.18
39-48	Cholesterol	Triglyceride	99.11
43-42	LDL	LDH	99.05
43-31	LDL	Amylase	99.03
36-20	HDL-C	MCHC	98.98
43-51	LDL	UA	98.86
36-31	HDL-C	Amylase	98.81
39-20	Cholesterol	MCHC	98.73
20-48	MCHC	Triglyceride	98.65
39-38	Cholesterol	Chlorine	98.62
43-38	LDL	Chlorine	98.43
20-31	MCHC	Amylase	98.28
36-42	HDL-C	LDH	98.16
48-42	Triglyceride	LDH	98.14

The resulting pairs contain the most effective features from the previous paragraph LDL (Nº43), Cholesterol (Nº39), HDL-C (Nº36), MCHC (Nº20), Triglyceride (Nº48), Amylase (Nº31), which have the best A_1 score (Table 7). The best result ($A_2 = 99.81$) was obtained

for the MCHC-MCH feature pair. At the same time, the pair contains the MCH(N₁₉) feature with low efficiency ($A_1 = 52.13$) and Pearson correlation ~ 0.041 . Such a combination of features with high and low correlation is observed very often, this combination results in a high classification efficiency. Among the features from Table 7, the following have a low linear correlation with the diagnosis: MCH (0.041), UA (0.066), Amylase (0.03), LDH (0.071), Pearson's coefficient is indicated in brackets.

There are pairs consisting entirely of effective features, for example, LDL-MCHC (N₄₃-N₂₀), HDL-C – MCHC (N₃₆-N₂₀), etc. Figure 4 shows the relationship between feature pairs for the top 50 -ty results. The main 6 features are located in the center. Asterisks indicate features that most often form a pair with the main features: UA (N₅₁), LDH (N₄₂), CK-MB (N₃₂), ALP (N₃₀). The main feature LDL (N₄₃) forms the largest number of effective pairs for classification.

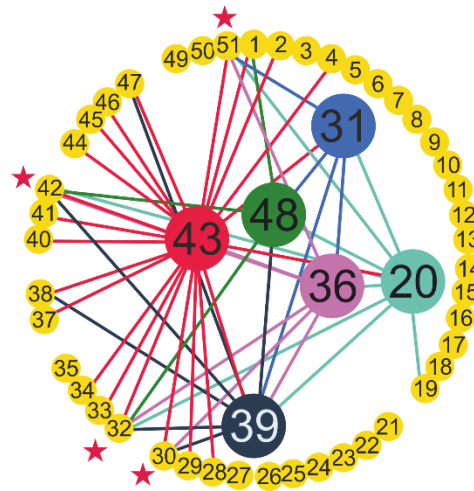
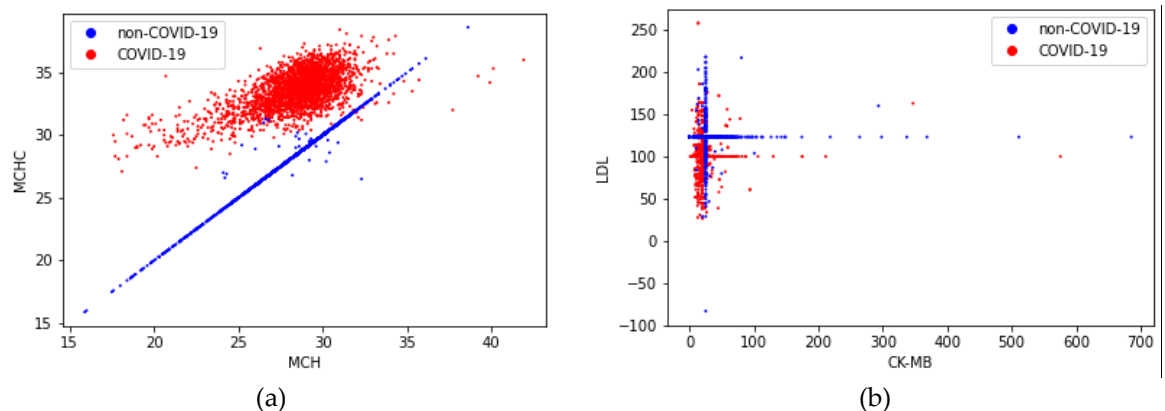


Figure 4. Pairs of features with high classification efficiency SARS-CoV-2-RBV1 datasets for the Histogram based Gradient Boosting classifier.

To find out the reasons for the effectiveness of pairs of features from Table 7, two-dimensional distributions of the diagnosis (attractors) were constructed for the first 6 pairs (Figure 5). It can be seen that for healthy patients (non-COVID-19) there are clear linear and cruciform attractors, while for people diagnosed with COVID-19, these attractors shift and become chaotic. This difference in the shape of the attractors allows classifiers to effectively distinguish between the two classes. The best separation of attractor shapes is observed for the MCHC-MCH pair (Figure 5a), which explains its highest classification ability. For the pairs in Figure 5b-e, shifted cruciform attractors are observed, which also contributes to their effective separation by classifiers. In Figure 5f, two attractors are blurred, but due to their weak intersection, the classification efficiency is high.



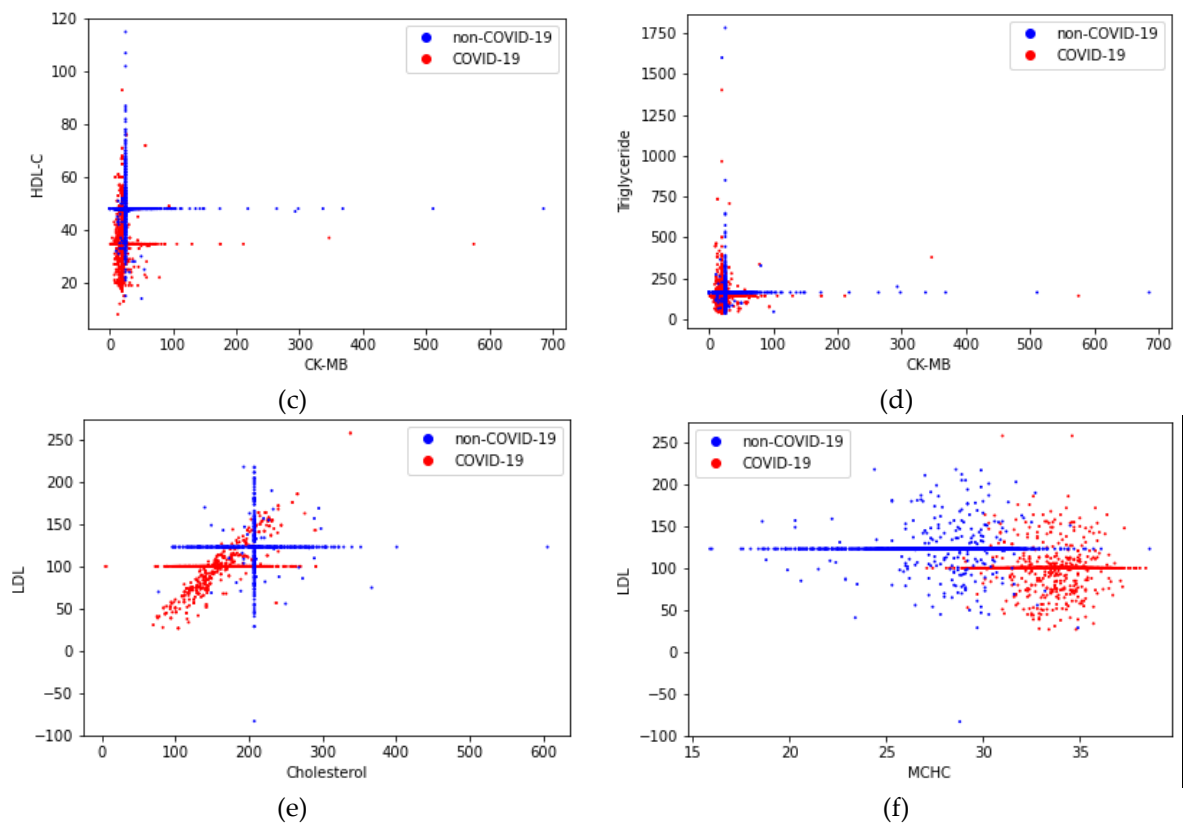


Figure 5. Two-dimensional distributions (attractors) of a COVID-19 and non-COVID-19 diagnosis in the coordinates of feature pairs a) MCHC—MCH, b) LDL—CK-MB, c) HDL—C-CK-MB, d) Triglyceride—CK-MB, e) LDL—Cholesterol, f) LDL—MCHC.

When using two features, the maximum accuracy is $A_2 = 99.81\%$ and it is less than when using the 51 features $A_{51} = 100\%$. However, feature reduction is important to simplify the classification of patients in practical terms. More accurate models can be obtained using three features.

The study of the most significant combination of 3 features of the HGB model.

Table 8 presents the classification result of SARS-CoV-2-RBV1 datasets for the HGB model using three input features.

Table 8. Classification efficiency of SARS-CoV-2-RBV1 datasets using 3 features for the Histogram based Gradient Boosting classifier.

№	First feature	Second feature	Third feature	Average accuracy $A_3, \%$
39-48-32	Cholesterol	Triglyceride	CK-MB	99.91
39-36-32	Cholesterol	HDL-C	CK-MB	99.91
43-20-19	LDL	MCHC	MCH	99.91
20-31-19	MCHC	Amylase	MCH	99.85
43-51-32	LDL	UA	CK-MB	99.85
39-20-19	Cholesterol	MCHC	MCH	99.83
48-42-32	Triglyceride	LDH	CK-MB	99.83
36-20-19	HDL-C	MCHC	MCH	99.79
36-42-32	HDL-C	LDH	CK-MB	99.79
43-38-51	LDL	Cholesterol	UA	99.79
20-48-19	MCHC	Triglyceride	MCH	99.77
39-48-31	Cholesterol	Triglyceride	Amylase	99.77

39-36-38	Cholesterol	HDL-C	Chlorine	99.75
36-31-51	HDL-C	Amylase	UA	99.75
39-36-42	Cholesterol	HDL-C	LDH	99.75
20-51-19	MCHC	UA	MCH	99.74
39-48-38	Cholesterol	Triglyceride	Chlorine	99.72
39-31-51	Cholesterol	Amylase	UA	99.70
39-48-42	Cholesterol	Triglyceride	LDH	99.66
48-31-42	Triglyceride	Amylase	LDH	99.51

An analysis of Table 8 shows that no new features have been added in the first twenty most accurate models compared to Table 7. It can also be seen that MCH and MCHC features are found only in pairs. With the addition of the third feature, the maximum classification efficiency increased from $A_2 = 99.81\%$ to $A_3 = 99.91\%$.

The study of the most significant combination of 11 features of the HGB model.

In tables 7 and 8, there are only 11 features: LDL (№43), Cholesterol (№39), HDL-C (№36), MCHC (№20), Triglyceride (№48), Amylase (№31), UA (№51), LDH (№42), CK-MB (№32), ALP (№30), MCH (№19). The classification accuracy of the HGB model using 11 features was $A_{11} = 100\%$. Thus, 11 features are sufficient to determine the diagnosis of the presence of coronavirus infection COVID-19 using machine learning methods using Histogram based Gradient Boosting classifier.

3.3. LogNet Implementation on Arduino for Edge Computing

A compact 77-line LogNet algorithm was created for diagnosing and predicting COVID-19 disease using routine blood values on an Arduino controller.

LogNet testing on Arduino revealed an accuracy of $A_{51} = 99.7\%$, which coincides with the accuracy on model computer program [36]. The input vector classification time is about 0.1 s.

An estimate of the used RAM of the Arduino controller is shown in Figure 6.

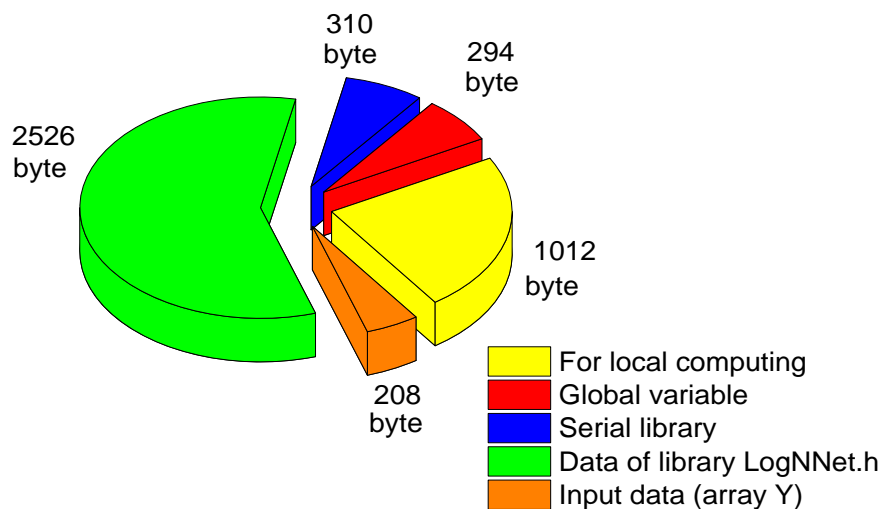


Figure 6. Estimation of the used RAM memory of the Arduino controller when working with the neural network LogNet 51:50:20:2.

Global variables (arrays S_h , S_{h2} and variables) occupy 294 bytes of RAM, incoming data is written to array Y which occupies 208 bytes. The Arduino uses the Serial system library to operate the serial port, it is loaded at initiation in the "void setup" block and takes up 310 bytes of RAM. The data stored in the LogNet.h library is also loaded into RAM during program initialization and takes 2526 bytes, the maximum contribution is

made by the matrix W_i - 2142 bytes. For local computations within functions and procedures, at least 1012 bytes must be reserved. The total RAM consumption is 4350 bytes.

3.4. Machine Learning COVID-19 Sensor for IoT

The LogNNNet network can be easily imported to various microcontrollers and can be used to predict a diagnosis based on blood biochemical parameters. Nevertheless, our experimental results in sections 3.2 and 3.3 show that it is significantly inferior in accuracy to resource-intensive machine learning algorithms. Therefore, we proposed two architectures of the IoT system (Figure 7), which includes an IoT device with LogNNNet implementation (edge computing) and a cloud service containing a trained HGB model (AI computing). These configurations implements the prognosis of the disease in offline and online modes and are ML sensors for diagnosis of COVID-19 disease (Sensor 1.0 type).

In the IoT device, data on the results of a biochemical blood test are entered manually or transmitted directly from the laboratory equipment. If the cloud service is unavailable or blood tests are performed on site using a mobile laboratory in remote areas, then the diagnosis is made using the LogNNNet network. If IoT device has access to the network infrastructure, it sends a network request to the cloud service, where the diagnosis is determined using the HGB model. The cloud service sends a response with a diagnosis, which is displayed on the IoT device using an LED indication or on an LCD display.

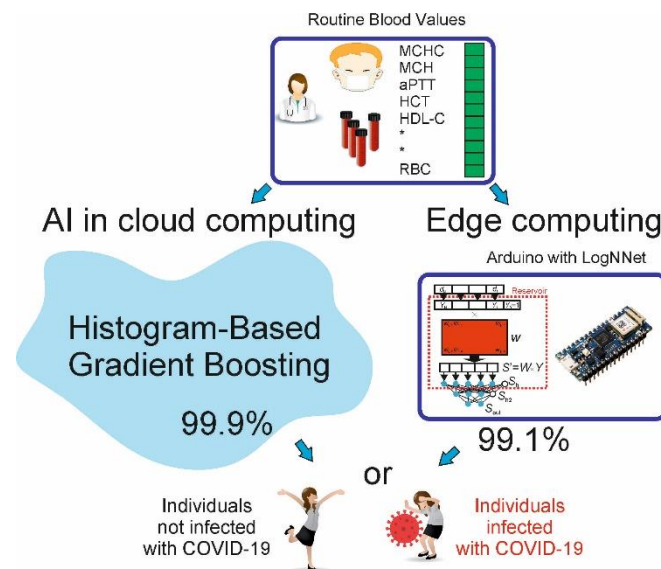


Figure 7. Two architectures of the IoT system, which includes an IoT device with LogNNNet implementation (edge computing) and a cloud service containing a trained HGB model (AI computing). The best classification accuracies are indicated for 3 features $A_3(\text{FS} [10,19,20]) = 99.169$ for LogNNNet [36] and $A_3(\text{FS} [39,48,32]) = 99.91$ for this research (Table 8).

4. Discussion

4.1 Analysis of results with a medical aspect

COVID-19 has attracted attention with its higher mortality and infectivity than influenza [3,14]. The disease still causes death and continues to spread [1,16,38]. The use of vaccines did not stop the spread of the disease, and important mutations were detected in the structure of the virus during the epidemic [1]. Most infected patients had mild symptoms and had a good prognosis. However, some patients developed severe symptoms such as severe pneumonia, acute respiratory distress syndrome (ARDS), and multiple organ dysfunction syndromes (MODS) [2,17,26]. However, there remains a need for studies to determine the prognosis and immune conditions of COVID-19 disease [3,70]. Therefore, early evaluation of patients who need intensive care and have high mortality expectations

and effective identification of relevant biomarkers are important to reduce the mortality of the disease [17,27,38].

Brinati et al. [43] and Zhang et al. [71] stated that various complications may be encountered during the treatment process of COVID-19 and therefore the course of the disease should be predicted earlier. Similarly, Mertoglu et al. [2] and Huyut and İlkbahar [17] stated that it is important to diagnose and predict the prognosis of the disease at an early stage so that the first response to severely infected COVID-19 patients can be done properly.

Although many studies on COVID-19 have been published, the relationships between the pathological aspects of the disease and routine blood values have not been fully determined [72]. Previous studies have reported that changes in many RBV and hematological abnormalities are observed during the course of the disease [15,72].

In this study, according to the A_{th} threshold classification result based on [36], the most effective features in the diagnosis of the disease were found to be LDL with 96.47%, HDL-C with 94.73%, Cholesterol with 94.47%, and MCHC with 94.35% (Table 3). Indeed, in previous studies, large changes in these features were reported in severe and fatal COVID-19 patients, and it was stated that they could be important biomarkers for the prognosis of the disease [1,2,15,17].

In the analysis performed by considering the linear dependency structures of the features among each other, the most effective combinations of dual features in the diagnosis of the disease were obtained and the Pearson correlation values were calculated (Table 4). The highly positive linear correlation structure of some trait pairs with positive and negative individuals was remarkable. Accordingly, the highest positive and negative linearly correlated trait pairs (high-high) were HCT-HGB, MPV-PDW, and HCT-RBC (96%, 93%, and 87%, respectively). It has been stated in previous studies that these features vary greatly in severe COVID-19 patients and may be associated with the prognosis and mortality of the disease [1,2,15]. The high positive association of trait pairs expressed as high-high type with both positive and negative COVID-19 individuals made us think that various comorbidities such as hypertension, obesity and diabetes may exist in our negative covid population. Furthermore, considering hospital admissions of negative COVID-19 patients, it appears that these trait pairs are highly associated not only with COVID-19 but also with various inflammatory syndromes and infections [1,2,73]. Djakpo et al. [74] stated that the abnormalities of HGB, HCT and RBC or anemia observed in patients with comorbidities are due to the inability of the bone marrow to produce enough RBCs to carry oxygen and lung damage caused by COVID-19 that complicates gas exchange.

On the other hand, considering the relationship of patients with these features, it is thought that the presence of possible comorbid conditions prevents erythrocyte production due to existing inflammation. Also, since the variation in these trait pairs is hypersensitive to the immune response in individuals, these trait pairs were highly correlated with sick and healthy individuals. It was seen that the MCH-MCHC trait pair was found to be highly positively correlated, especially with healthy individuals, and this pair could be used as important markers to distinguish healthy individuals in the diagnosis of the disease. Indeed Mertoğlu et al. [1] stated that changes in these characteristics may indicate suppression of lymphocytic and erythrocyte series or platelet and erythrocyte deformities. Also, in this study, a highly positive association of the MCH-MCV trait pair with COVID-19 was found. Mertoğlu et al. [2] Huyut et al. [15] Karakike et al [23] stated that this was due to the decrease in the size of erythrocytes and anisocytosis in patients. In addition, the high positive association of HGB-RBC trait pair with sick individuals may be related to impaired erythropoiesis in the later stages of the disease. The high-high type feature set provides important clues in the isolation of both sick and healthy individuals.

In Table 4, a high (77%) negative relationship between the fibrinogen-LYM feature pair and covid patients is seen, and we think that this level of relationship is due to the fibrinogen feature. Indeed, Winata and Kurniawan [30] noted that the degradation product of fibrinogen (FBU) was increased in all patients in the late stage of COVID-19 and

that this was significantly associated with coagulation. In addition, the high correlation of Cholesterol-LDL, Cholesterol-HDL-C and Chlorine-Sodium trait pairs (High-low type in Table 4) with sick individuals showed that these trait pairs were important markers in identifying sick individuals. Fang et al. [75], Mertoğlu et al. [1] stated that this feature set may be associated with multi-organ involvement in COVID-19 and the widespread distribution of angiotensin-converting enzyme receptors in the body.

The fact that low-high trait pairs MCHC-MCV was found to be highly positively correlated with covid negative individuals in Table 4 suggested the importance of the size of erythrocyte and anisocytosis in healthy individuals [75]. In addition, the functional properties of ALT-AST, eGFR-Urea, and D-Bil-T-Bil pairs were found to be important markers in the isolation of individuals with negative covid. As a matter of fact, Mertoğlu et al. [1], Huyut et al. [15], Zhou et al. [29] stated that the decrease in ALT, AST, GGT, total bilirubin, and eGFR indicated that the patients had serious damage to organs such as pancreas and kidney. In another study, Bertolini et al. [76] stated that AST, GGT, ALP and bilirubin may be frequently elevated in COVID-19 and that the main underlying causes of this condition may be hyper inflammation and thrombotic microangiopathy. In addition, the high positive correlation of INR-PT trait pair with negative covid individuals suggested that it is important to monitor these individuals for the development of disseminated intravascular coagulopathy and acute respiratory distress [75,77].

In this study, 13 popular classifier machine learning models and LogNNet neural network model were run on 51 routine blood values to detect patients infected with COVID-19. Histogram based Gradient Boosting was the model with the fastest and highest accuracy in determining the diagnosis of the disease (accuracy: 100%, time: 6.39 sec). For the HGB model using a single input feature (A_1), the most effective features in the diagnosis of the disease were found LDL 96.87% (№43), Cholesterol 95.07% (№39), HDL-C 94.99% (№36), MCHC 94.35% (№20), Triglyceride (№48), Amylase (№31) (Table 6). For the HGB model using the dual entry feature (A_2), the most effective trait pair MCHC-MCH was found in the diagnosis of the disease ($A_2 = 99.81$) (Table 7). The success of MCH as a single entry feature in the diagnosis of the disease is low ($A_1 = 52.13$). Huyut and Velichko [36] found an accuracy rate of 99.1% in the diagnosis of the disease by running the MCHC-MCH features with LogNNet. Accordingly, the HGB model operated with MCHC-MCH was found to be more successful than the LogNNet model in the diagnosis of the disease.

Since it was stated in previous studies [78] that low values of MCH and high values of MCHC were associated with COVID-19, it was expected that the use of these two features together in the diagnosis of the disease would produce much higher classification success. The most effective dual trait pairs (Table 7) were similar to the most effective single traits (Table 6) for the HGB model at diagnosis of the disease. This suggested that it provides important information about the functional properties of the binary trait pairs obtained with the HGB model in the diagnosis of the disease. 6 basic features (LDL (№43), Cholesterol (№39), HDL-C (№36), MCHC (№20), Triglyceride (№48), Amylase (№31) among the combinations of binary features used in the diagnosis of the disease and the 4 features UA (№51), LDH (№42), CK-MB (№32), ALP (№30) that most frequently pair with these features are given in Figure 4. The main feature LDL (№43) generated the largest number of effective pairs for classification. The effectiveness of these feature pairs (Table 7) in detecting patients is visualized in two-dimensional space (Figure 5). Figure 5a, where classification is most clearly visible, was the MCHC-MCH pair, which explains the highest classification ability.

In the binary feature combinations used by HGB in the diagnosis of the disease, the maximum accuracy was found to be $A_2 = 99.81\%$ and slightly lower than the use of 51 features ($A_{51} = 100\%$). However, feature reduction provides more economical and rapid results in interpreting the classification of patients from a practical point of view and identifying the most effective features.

The highest classification success obtained for the HGB model using three feature combinations was found to be $A_3 = 99.91$ (Table 8).

Analysis of Table 8 showed that no new features were added to the top twenty models with the highest accuracy compared to Table 7. This showed that the binary combinations in Table 7 were sufficient for the diagnosis of the disease. In addition, the co-existence of MCH and MCHC features in all combinations supported that there are hidden association structures between these features (see also Figure 5a) and that they contain important clues in the diagnosis of the disease.

In this study, the most important 11 biomarkers were found with the HGB model used to determine the diagnosis of the disease, and with these features, all patients and healthy individuals were correctly identified with high performance ($A_{11} = 100\%$). In addition, the importance of various combinations of these features in the diagnosis of the disease was recognized. The performance of these 11 features (LDL (№43), Cholesterol (№39), HDL-C (№36), MCHC (№20), Triglyceride (№48), Amylase (№31), UA (№51), LDH (№42), CK-MB (№32), ALP (№30), MCH (№19) and their various combinations in the diagnosis of the disease was higher than the individual performances, suggesting that there is a high level of confidential information between these feature combinations and COVID-19.

Kocar et al. [79] and Zinellu et al. [80] presented evidence of significant changes in the lipid profile of severe COVID19 patients, particularly in total cholesterol, LDL, cholesterol, and HDL-C concentrations. They also reported that increased cholesterol concentrations in the cell membrane increased the binding activity of SARS-CoV-2, facilitated membrane fusion, and enabled successful entry of the virus into the host. Therefore, Kocar et al. [79] and Wei et al. [81] indicate that total cholesterol, LDL, and HDL-C characteristics may aid in early risk stratification and clinical decisions. However, conflicting results have been reported for changes in Triglyceride levels of severe COVID-19 patients [80]. Stephens et al. [82] stated that in severe COVID-19 patients, the elevated serum amylase value is often not attributable to acute pancreatitis or a clinically significant pancreatic injury, but is more likely to be a nonspecific manifestation of shock/critical illness. Mao et al. [78] stated that changes in Leukocytes, neutrophils, lymphocytes, platelets, hemoglobin levels, MCV and MCHC are generally associated with lung involvement, oxygen demand and disease activity. They also noted that high MCV and low MCHC are associated with advanced anemia and are independent predictors of disease worsening [78].

Wu et al. [83] stated that an increase or decrease in LDH is indicative of radiographic progression or improvement. They also demonstrated the potential usefulness of serum LDH as a marker for assessing clinical severity, monitoring treatment response, and thus aiding risk stratification and early intervention in COVID-19 pneumonia. Hu et al. [84] stated that SARS-CoV-2 infection is associated with low serum uric acid (SUA) levels and this feature may be an independent risk factor for the diseases. They also noted that male patients with COVID-19 accompanied by low SUA levels are at higher risk of developing severe symptoms than those with high SUA levels at admission. Zinellu et al. [85] found that high CK-MB concentrations were significantly associated with severe morbidity and mortality in COVID-19 patients. They stated that this biomarker of myocardial damage may be useful for the classification of patients with severe covid, and that high CK-MB values may reflect excessive inflammation status. They also stated that the evaluation of CK-MB in COVID-19 patients provides specific clinical information for early risk stratification, independent of myocardial necrosis and cardiac complications. Afra et al. [86] showed the incidence of abnormal liver tests in severe COVID-19 patients and reported the association of elevated AST, ALT and total Bilirubin levels with liver injury in severe COVID-19 patients [14,86,87]. However, conflicting results have been reported regarding the ALP levels of mild and severe COVID-19 patients [86]. In addition, Afra et al [86] showed that elevated liver enzymes can effectively predict hospital-critical covid cases.

4.1 Analysis of results with IoT aspect

The proposed solution shows the LogNNNet network can be easily imported to various microcontrollers. As a generic result, many IoT devices can be made smarter, so opening a way to develop advanced Aml healthcare with essential part of IoT and edge intelligence [88]. Our conclusion is that such LogNNNet-equipped ML sensor can take a worthy share in future IoT applications for healthcare and for some other problem domains with active digitalization and emerging Aml methods [9].

The LogNNNet network can be used to predict a diagnosis based on blood biochemical parameters. We expect that this result is an important step in smart human sensorics for IoT application, since the COVID-19 status and other blood-related health parameters are not easy to analyze in the IoT edges (in contrast to more widespread parameters such as temperature or heartbeat). Our conclusion is that the approach is applicable to development of personalized bionic systems (smart suit for a person or Aml environment with people) where disease status recognition (e.g., COVID-19 as in our case) is a regular digital service for healthcare or well-being in everyday life [8].

We understand that small IoT devices cannot provide such high accuracy as resource-intensive ML algorithms on powerful computer systems. Nevertheless, AAL systems are intended for the active use in everyday life settings (e.g., at home, workspace, outdoor). Exact medical- grounded decisions with strong support are not the goal in this AAL case, instead, attention points and optional recommendations for the personal use are the result of digital services. Such services assist to the person; they do not require mandatory actions to perform. We think, that this type of human sensorics is expected to move from the very restricted medical lab setting toward the wide market of smart consumer electronics and digital services [9].

5. Conclusions

Determining the COVID-19 infected status with various diagnostic tests and imaging results is costly and time-consuming. In addition, if this process is prolonged, the patient's health may be at greater risk by being exposed to different complications. This study provides a fast, reliable and economical alternative mobile tool for the diagnosis of COVID-19 based on the RBV values measured at the time of admission.

In this study, 13 popular classifier machine learning models and LogNNNet neural network model were run on 51 routine blood values to detect patients infected with COVID-19. Histogram-based Gradient Boosting model was the most successful classification model in terms of accuracy and time in detecting the diagnosis of the disease (accuracy: 100%, time: 6.39 sec). In addition, the absence of any normalization method and additional feature selection procedure for the HGB model was seen as a faster and more economical advantage of this model.

In this study, the 11 most important biomarkers in the diagnosis of the disease were found with the HGB classifier. These features are; LDL (№43), Cholesterol (№39), HDL-C (№36), MCHC (№20), Triglyceride (№48), Amylase (№31), UA (№51), LDH (№42), CK-MB (№32), ALP (№30), MCH (№19). Using only these 11 RBV features, the HGB model accurately detected all COVID-19 patients ($A_{11} = 100\%$).

The high accuracy rate of the single, double and triple combinations of these 11 features selected by the HGB model in the diagnosis of the disease showed the importance of these features in the diagnosis of the disease. In addition, the performance of double and triple combinations of these features in the detection of sick and healthy individuals was higher than the individual performances, suggesting that there is a high level of confidential information between these blood feature combinations and COVID-19.

It can be said that 11 features are sufficient for the diagnosis of the presence of COVID-19 using the HGB classifier. This information was revealed by the HGB model. As described by the HGB model, these features and their binary combinations are an important source of variation in the diagnosis of COVID-19. We propose to use these features

and their binary combinations to be run with HGB as important biomarkers in the diagnosis of the disease.

In addition, the results of this study can be effectively used in IoT(IoTM) medical edge devices with low RAM resources, ML sensors, portable point-of-care blood testing devices [89], clinical decision support systems, remote internet medicine and telemedicine. The experimental results showed the feasibility of using ML sensors in AAL systems.

Author Contributions: Conceptualization, M.T.H., and A.V.; methodology, A.V., M.T.H., M.B., Y.I. and D.K.; software, A.V., M.T.H., M.B. and Y.I.; validation, M.T.H. and A.V.; formal analysis, A.V., M.T.H., M.B., Y.I. and D.K.; investigation, A.V.; resources, M.T.H.; data curation, M.T.H.; writing—original draft preparation, A.V., M.T.H., M.B., Y.I. and D.K.; writing—review and editing, A.V., M.T.H., M.B., Y.I. and D.K.; visualization, A.V. and M.B.; supervision, D.K.; project administration, D.K.; funding acquisition, D.K. All authors have read and agreed to the published version of the manuscript.

Funding: The research is implemented with financial support by Russian Science Foundation, project no. 22-11-20040 (<https://rscf.ru/en/project/22-11-20040/>) jointly with Republic of Karelia and funding from Venture Investment Fund of Republic of Karelia (VIF RK).

Institutional Review Board Statement: The dataset used in this study was collected in order to be used in various studies in the estimation of the diagnosis, prognosis and mortality of COVID-19. The necessary permissions for the collected dataset were given by the Ministry of Health of the Republic of Turkey and the Ethics Committee of Erzincan Binali Yıldırım University. This study was conducted in accordance with the 1989 Declaration of Helsinki. Erzincan Binali Yıldırım University Human Research Health and Sports Sciences Ethics Committee Decision Number: 2021/02-07.

Informed Consent Statement: In this study, a dataset including only routine blood values, RT-PCR results (positive or negative) and treatment units of the patients was downloaded retrospectively from the information system of our hospital in digital environment. A new sample was not taken from the patients. There is no information in the dataset that includes identifying characteristics of individuals. It was stated that routine blood values would only be used in academic studies, and written consent was obtained from the institutions for this. In addition, therefore, written informed consent was not administered for every patient.

Data Availability Statement: The data used in this study can be shared with the parties, provided that the article is cited.

Acknowledgments: We thank the method of Erzincan Mengücek Gazi Training and Research Hospital for their support in reaching the material used in this study. Special thanks to the editors of the journal and to the anonymous reviewers for their constructive criticism and improvement suggestions.

Conflicts of Interest: The authors declare no conflict of interest.

Appendix A

Algorithm A1. LogNNet neural network executable code on Arduino Nano IoT 33.

```

1 #include "LogNNet.h"
2
3 float Y[S+1];
4 float Sh[P+1];
5 float Sh2[M+1];
6
7 int i = 0;
8 String data;
9
10 float Fun_activ(float x) {
11     return 1 / (1 + exp(-1*x));
12 }
13
14 void Reservoir(float *Y) {
15     long W = C;
16     Sh[0] = 1;
17     for (int j = 1; j <= P; j++) {
18         Sh[j] = 0;
19         for (int i = 0; i <= S; i++) {
20             W = (D - K * W) % L;
21             Sh[j] = Sh[j] + ((float)W/L) * Y[i];
22         }
23         Sh[j] = ((Sh[j] - (float)minS[j-1]/
24             scale_factor) / ((float)(maxS[j-1]
25             - minS[j-1])/scale_factor)) - 0.5
26             - (float)meanS[j-1]/(scale_factor*10);
27     }
28 }
29
30 void Hidden_Layer() {
31     Sh2[0] = 1;
32     for (int j = 1; j <= M; j++) {
33         Sh2[j] = 0;
34         for (int i = 0; i <= P; i++)
35             Sh2[j] = Sh2[j] + Sh[i] *
36                 ((float)W1[i][j]/scale_factor);
37         Sh2[j] = Fun_activ(Sh2[j]);
38     }
39 }
40
41 byte Output_Layer() {
42     float Sout[N+1]; byte digit = 0;
43     for (int j = 0; j <= N; j++) {
44         Sout[j] = 0;
45         for (int i = 0; i <= M; i++)
46             Sout[j] = Sout[j] + Sh2[i] *
47                 ((float)W2[i][j]/scale_factor);
48         Sout[j] = Fun_activ(Sout[j]);
49     }
50     for (int j = 0; j <= N; j++) {
51         if (Sout[j] > Sout[digit])
52             digit = j;
53     }
54     return digit;
55 }
56
57 void setup() {
58     Serial.begin(115200);
59 }
60
61 void loop() {
62     if (Serial.available() > 0) {
63         data = Serial.readStringUntil('T');
64
65         if (data != "FN") {
66             Y[i] = data.toFloat();
67             i++;
68         }
69         else {
70             i = 0;
71             Reservoir(Y);
72             Hidden_Layer();
73             byte Digit = Output_Layer();
74             Serial.print(String(Digit));
75         }
76     }
77 }

```

References

1. Mertoglu, C.; Huyut, M.; Olmez, H.; Tosun, M.; Kantarci, M.; Coban, T. COVID-19 Is More Dangerous for Older People and Its Severity Is Increasing: A Case-Control Study. *Med. Gas Res.* **2022**, *12*, 51–54, doi:10.4103/2045-9912.325992.
2. Mertoglu, C.; Huyut, M.T.; Arslan, Y.; Ceylan, Y.; Coban, T.A. How Do Routine Laboratory Tests Change in Coronavirus Disease 2019? *Scand. J. Clin. Lab. Invest.* **2021**, *81*, 24–33, doi:10.1080/00365513.2020.1855470.
3. Zhou, C.; Chen, Y.; Ji, Y.; He, X.; Xue, D. Increased Serum Levels of Hepcidin and Ferritin Are Associated with Severity of COVID-19. *Med. Sci. Monit.* **2020**, *26*, 1–6, doi:10.12659/MSM.926178.
4. HUYUT, M.T.; HUYUT, Z. Forecasting of Oxidant/Antioxidant Levels of COVID-19 Patients by Using Expert Models with Biomarkers Used in the Diagnosis/Prognosis of COVID-19. *Int. Immunopharmacol.* **2021**, *100*, doi:10.1016/j.intimp.2021.108127.
5. Meigal, A.Y.; Korzun, D.G.; Moschevikin, A.P.; Reginya, S.; Gerasimova-Meigal, L.I. Ambient Assisted Living At-Home Laboratory for Motor Status Diagnostics in Parkinson's Disease Patients and Aged People. <https://services.igi-global.com/resolvedoi/resolve.aspx?doi=10.4018/978-1-6684-5295-0.ch047> **1AD**, 836–862, doi:10.4018/978-1-6684-5295-0.CH047.
6. Fernandes, J.M.; Silva, J.S.; Rodrigues, A.; Boavida, F. A Survey of Approaches to Unobtrusive Sensing of Humans. *ACM Comput. Surv.* **2022**, *55*, doi:10.1145/3491208.
7. Kostakos, V.; Rogstadius, J.; Ferreira, D.; Hosio, S.; Goncalves, J. Human Sensors BT - Participatory Sensing, Opinions and Collective Awareness. In: Loreto, V., Haklay, M., Hotho, A., Servedio, V.D.P., Stumme, G., Theunis, J., Tria, F., Eds.; Springer International Publishing: Cham, 2017; pp. 69–92 ISBN 978-3-319-25658-0.
8. Korzun, D.G. Internet of Things Meets Mobile Health Systems in Smart Spaces: An Overview BT - Internet of Things and Big Data Technologies for Next Generation Healthcare. In: Bhatt, C., Dey, N., Ashour, A.S., Eds.; Springer International Publishing: Cham, 2017; pp. 111–129 ISBN 978-3-319-49736-5.
9. Korzun, D.; Balandina, E.; Kashevnik, A.; Balandin, S.; Viola, F. *Ambient Intelligence Services in IoT Environments*; 2019; ISBN 9781522589730.
10. Warden, P.; Stewart, M.; Plancher, B.; Banbury, C.; Prakash, S.; Chen, E.; Asgar, Z.; Katti, S.; Reddi, V.J. Machine Learning Sensors. **2022**, doi:10.48550/arxiv.2206.03266.
11. Chinchole, S.; Patel, S. Artificial Intelligence and Sensors Based Assistive System for the Visually Impaired People. In Proceedings of the 2017 International Conference on Intelligent Sustainable Systems (ICISS); 2017; pp. 16–19.
12. Gulzar Ahmad, S.; Iqbal, T.; Javaid, A.; Ullah Munir, E.; Kirn, N.; Ullah Jan, S.; Ramzan, N. Sensing and Artificial Intelligent Maternal-Infant Health Care Systems: A Review. *Sensors* **2022**, *22*.
13. Machine Learning Sensors: Truly Data-Centric AI | Towards Data Science Available online: <https://towardsdatascience.com/machine-learning-sensors-truly-data-centric-ai-8f6b9904633a> (accessed on 23 August 2022).
14. Chen, N.; Zhou, M.; Dong, X.; Qu, J.; Gong, F.; Han, Y.; Qiu, Y.; Wang, J.; Liu, Y.; Wei, Y.; et al. Epidemiological and Clinical Characteristics of 99 Cases of 2019 Novel Coronavirus Pneumonia in Wuhan, China: A Descriptive Study. *Lancet* **2020**, *395*, 507–513, doi:10.1016/S0140-6736(20)30211-7.
15. Tahir Huyut, M.; Huyut, Z.; İlkbahar, F.; Mertoğlu, C. What Is the Impact and Efficacy of Routine Immunological, Biochemical and Hematological Biomarkers as Predictors of COVID-19 Mortality? *Int. Immunopharmacol.* **2022**, *105*, doi:10.1016/j.intimp.2022.108542.
16. Huyut, M.T.; Kocaturk, İ. The Effect of Some Symptoms and Features During the Infection Period on the Level of Anxiety and Depression of Adults After Recovery From COVID-19. *Curr. Psychiatry Res. Rev.* **2022**, *18*, doi:10.2174/2666082218666220325105504.
17. Huyut, M.T.; İlkbahar, F. The Effectiveness of Blood Routine Parameters and Some Biomarkers as a Potential Diagnostic Tool in the Diagnosis and Prognosis of Covid-19 Disease. *Int. Immunopharmacol.* **2021**, *98*, doi:10.1016/j.intimp.2021.107838.
18. Guan, W.; Ni, Z.; Hu, Y.; Liang, W.; Ou, C.; He, J.; Liu, L.; Shan, H.; Lei, C.; Hui, D.S.C.; et al. Clinical Characteristics of

- Coronavirus Disease 2019 in China. *N. Engl. J. Med.* **2020**, *382*, 1708–1720, doi:10.1056/nejmoa2002032.
19. Banerjee, A.; Ray, S.; Vorselaars, B.; Kitson, J.; Mamalakis, M.; Weeks, S.; Baker, M.; Mackenzie, L.S. Use of Machine Learning and Artificial Intelligence to Predict SARS-CoV-2 Infection from Full Blood Counts in a Population. *Int. Immunopharmacol.* **2020**, *86*, doi:10.1016/j.intimp.2020.106705.
 20. Huyut, M.T.; Soygüder, S. The Multi-Relationship Structure between Some Symptoms and Features Seen during the New Coronavirus 19 Infection and the Levels of Anxiety and Depression Post-Covid. *East. J. Med.* **2022**, *27*, doi:10.5505/ejm.2022.35336.
 21. Perricone, C.; Bartoloni, E.; Bursi, R.; Cafaro, G.; Guidelli, G.M.; Shoenfeld, Y.; Gerli, R. COVID-19 as Part of the Hyperferritinemic Syndromes: The Role of Iron Depletion Therapy. *Immunol. Res.* **2020**, *68*, 213–224, doi:10.1007/s12026-020-09145-5.
 22. Mehta, P.; McAuley, D.F.; Brown, M.; Sanchez, E.; Tattersall, R.S.; Manson, J.J. COVID-19: Consider Cytokine Storm Syndromes and Immunosuppression. *Lancet* **2020**, *395*, 1033–1034, doi:10.1016/S0140-6736(20)30628-0.
 23. Karakike, E.; Giamarellos-Bourboulis, E.J. Macrophage Activation-like Syndrome: A Distinct Entity Leading to Early Death in Sepsis. *Front. Immunol.* **2019**, *10*, doi:10.3389/fimmu.2019.00055.
 24. Tural Onur, S.; Altın, S.; Sokucu, S.N.; Fikri, B.İ.; Barça, T.; Bolat, E.; Toptaş, M. Could Ferritin Level Be an Indicator of COVID-19 Disease Mortality? *J. Med. Virol.* **2021**, *93*, 1672–1677, doi:10.1002/jmv.26543.
 25. Rosário, C.; Zandman-Goddard, G.; Meyron-Holtz, E.G.; D’Cruz, D.P.; Shoenfeld, Y. The Hyperferritinemic Syndrome: Macrophage Activation Syndrome, Still’s Disease, Septic Shock and Catastrophic Antiphospholipid Syndrome. *BMC Med.* **2013**, *11*, doi:10.1186/1741-7015-11-185.
 26. Lippi, G.; Plebani, M.; Henry, B.M. Thrombocytopenia Is Associated with Severe Coronavirus Disease 2019 (COVID-19) Infections: A Meta-Analysis. *Clin. Chim. Acta* **2020**, *506*, 145–148, doi:10.1016/j.cca.2020.03.022.
 27. Cheng, L.; Li, H.; Li, L.; Liu, C.; Yan, S.; Chen, H.; Li, Y. Ferritin in the Coronavirus Disease 2019 (COVID-19): A Systematic Review and Meta-Analysis. *J. Clin. Lab. Anal.* **2020**, *34*, 1–18, doi:10.1002/jcla.23618.
 28. Feld, J.; Tremblay, D.; Thibaud, S.; Kessler, A.; Naymagon, L. Ferritin Levels in Patients with COVID-19: A Poor Predictor of Mortality and Hemophagocytic Lymphohistiocytosis. *Int. J. Lab. Hematol.* **2020**, *42*, 773–779, doi:10.1111/ijlh.13309.
 29. Zhou, F.; Yu, T.; Du, R.; Fan, G.; Liu, Y.; Liu, Z.; Xiang, J.; Wang, Y.; Song, B.; Gu, X.; et al. Clinical Course and Risk Factors for Mortality of Adult Inpatients with COVID-19 in Wuhan, China: A Retrospective Cohort Study. *Lancet* **2020**, *395*, 1054–1062, doi:10.1016/S0140-6736(20)30566-3.
 30. Winata, S.; Kurniawan, A. Coagulopathy in COVID-19: A Systematic Review. *Medicus* **2021**, *8*, 72, doi:10.19166/med.v8i2.3444.
 31. Hariyanto, T.I.; D, M.; Japar, K.V.; D, M.; Kwenandar, F.; D, M.; Damay, V.; D, M.; Siregar, J.I.; D, M.; et al. Since January 2020 Elsevier Has Created a COVID-19 Resource Centre with Free Information in English and Mandarin on the Novel Coronavirus COVID-19. The COVID-19 Resource Centre Is Hosted on Elsevier Connect, the Company’s Public News and Information. **2020**.
 32. Amgalan, A.; Othman, M. Hemostatic Laboratory Derangements in COVID-19 with a Focus on Platelet Count. *Platelets* **2020**, *31*, 740–745, doi:10.1080/09537104.2020.1768523.
 33. Kukar, M.; Gunčar, G.; Vovko, T.; Podnar, S.; Černelč, P.; Brvar, M.; Zalaznik, M.; Notar, M.; Moškon, S.; Notar, M. COVID-19 Diagnosis by Routine Blood Tests Using Machine Learning. *Sci. Rep.* **2021**, *11*, 10738, doi:10.1038/s41598-021-90265-9.
 34. Jiang, S.Q.; Huang, Q.F.; Xie, W.M.; Lv, C.; Quan, X.Q. The Association between Severe COVID-19 and Low Platelet Count: Evidence from 31 Observational Studies Involving 7613 Participants. *Br. J. Haematol.* **2020**, *190*, e29–e33, doi:10.1111/bjh.16817.
 35. Zheng, Y.; Zhang, Y.; Chi, H.; Chen, S.; Peng, M.; Luo, L.; Chen, L.; Li, J.; Shen, B.; Wang, D. The Hemocyte Counts as a Potential Biomarker for Predicting Disease Progression in COVID-19: A Retrospective Study. *Clin. Chem. Lab. Med.* **2020**, *58*, 1106–1115, doi:10.1515/cclm-2020-0377.

36. Huyut, M.T.; Velichko, A. Diagnosis and Prognosis of COVID-19 Disease Using Routine Blood Values and LogNNet Neural Network. *Sensors* **2022**, *22*, 4820, doi:10.3390/s22134820.
37. Huyut, M.T. Automatic Detection of Severely and Mildly Infected COVID-19 Patients with Supervised Machine Learning Models. *IRBM* **2022**, *1*, 1–12, doi:10.1016/j.irbm.2022.05.006.
38. Huyut, M.; Üstündağ, H. Prediction of Diagnosis and Prognosis of COVID-19 Disease by Blood Gas Parameters Using Decision Trees Machine Learning Model: A Retrospective Observational Study. *Med. Gas Res.* **2022**, *12*, 60–66, doi:10.4103/2045-9912.326002.
39. Li, X.; Wang, L.; Yan, S.; Yang, F.; Xiang, L.; Zhu, J.; Shen, B.; Gong, Z. Clinical Characteristics of 25 Death Cases with COVID-19: A Retrospective Review of Medical Records in a Single Medical Center, Wuhan, China. *Int. J. Infect. Dis.* **2020**, *94*, 128–132, doi:10.1016/j.ijid.2020.03.053.
40. Beck, B.R.; Shin, B.; Choi, Y.; Park, S.; Kang, K. Predicting Commercially Available Antiviral Drugs That May Act on the Novel Coronavirus (SARS-CoV-2) through a Drug-Target Interaction Deep Learning Model. *Comput. Struct. Biotechnol. J.* **2020**, *18*, 784–790, doi:10.1016/j.csbj.2020.03.025.
41. Xu, X.; Jiang, X.; Ma, C.; Du, P.; Li, X.; Lv, S.; Yu, L.; Ni, Q.; Chen, Y.; Su, J.; et al. A Deep Learning System to Screen Novel Coronavirus Disease 2019 Pneumonia. *Engineering* **2020**, *6*, 1122–1129, doi:10.1016/j.eng.2020.04.010.
42. Gupta, V.K. Crime Tracking System and People ' s Safety in India Using Machine Learning Approaches. **2022**, *2*, 1–7.
43. Brinati, D.; Campagner, A.; Ferrari, D.; Locatelli, M.; Banfi, G.; Cabitza, F. Detection of COVID-19 Infection from Routine Blood Exams with Machine Learning: A Feasibility Study. *J. Med. Syst.* **2020**, *44*, doi:10.1007/s10916-020-01597-4.
44. Chatterjee, I. Patenting Machine-Learning: Review and Discussions. *Int. J. Mod. Res.* **2021**, *1*, 15–21.
45. Cabitza, F.; Campagner, A.; Ferrari, D.; Di Resta, C.; Ceriotti, D.; Sabetta, E.; Colombini, A.; De Vecchi, E.; Banfi, G.; Locatelli, M.; et al. Development, Evaluation, and Validation of Machine Learning Models for COVID-19 Detection Based on Routine Blood Tests. *Clin. Chem. Lab. Med.* **2021**, *59*, 421–431, doi:10.1515/cclm-2020-1294.
46. Remeseiro, B.; Bolon-Canedo, V. A Review of Feature Selection Methods in Medical Applications. *Comput. Biol. Med.* **2019**, *112*, 103375, doi:https://doi.org/10.1016/j.combiomed.2019.103375.
47. Bikku, T. Multi-Layered Deep Learning Perceptron Approach for Health Risk Prediction. *J. Big Data* **2020**, *7*, doi:10.1186/s40537-020-00316-7.
48. Battineni, G.; Chintalapudi, N.; Amenta, F. Machine Learning in Medicine: Performance Calculation of Dementia Prediction by Support Vector Machines (SVM). *Informatics Med. Unlocked* **2019**, *16*, 100200, doi:https://doi.org/10.1016/j.imu.2019.100200.
49. Xing, W.; Bei, Y. Medical Health Big Data Classification Based on KNN Classification Algorithm. *IEEE Access* **2020**, *8*, 28808–28819, doi:10.1109/ACCESS.2019.2955754.
50. Hoodbhoy, Z.; Noman, M.; Shafique, A.; Nasim, A.; Chowdhury, D.; Hasan, B. Use of Machine Learning Algorithms for Prediction of Fetal Risk Using Cardiotocographic Data. *Int. J. Appl. Basic Med. Res.* **2019**, *9*, 226, doi:10.4103/ijabmr.ijabmr_370_18.
51. Alam, M.Z.; Rahman, M.S.; Rahman, M.S. A Random Forest Based Predictor for Medical Data Classification Using Feature Ranking. *Informatics Med. Unlocked* **2019**, *15*, 100180, doi:https://doi.org/10.1016/j.imu.2019.100180.
52. Schober, P.; Vetter, T.R. Logistic Regression in Medical Research. *Anesth. Analg.* **2021**, 365–366.
53. Podgorelec, V.; Kokol, P.; Stiglic, B.; Rozman, I. Decision Trees: An Overview and Their Use in Medicine. *J. Med. Syst.* **2002**, *26*, 445–463, doi:10.1023/A:1016409317640.
54. Guyon, I.; Gunn, S.; Nikravesh, M.; Zadeh, L.A. *Feature Extraction: Foundations and Applications*; Studies in Fuzziness and Soft Computing; Springer Berlin Heidelberg, 2008; ISBN 9783540354888.
55. Hall, M.A. Correlation-Based Feature Selection for Machine Learning. **1999**.
56. Dash, M.; Liu, H. Consistency-Based Search in Feature Selection. *Artif. Intell.* **2003**, *151*, 155–176, doi:10.1016/S0004-

3702(03)00079-1.

57. Zhao, Z.; Liu, H. Searching for Interacting Features. *IJCAI Int. Jt. Conf. Artif. Intell.* **2007**, 1156–1161.
58. Hall, M.A.; Smith, L.A. Practical Feature Subset Selection for Machine Learning 1998, *Volume 20*, 181–191.
59. Kononenko, I. Estimating Attributes: Analysis and Extensions of RELIEF. *Lect. Notes Comput. Sci. (including Subser. Lect. Notes Artif. Intell. Lect. Notes Bioinformatics)* **1994**, 784 LNCS, 171–182, doi:10.1007/3-540-57868-4_57.
60. Le Thi, H.A.; Nguyen, V.V.; Ouchani, S. Gene Selection for Cancer Classification Using DCA. *Lect. Notes Comput. Sci. (including Subser. Lect. Notes Artif. Intell. Lect. Notes Bioinformatics)* **2008**, 5139 LNAI, 62–72, doi:10.1007/978-3-540-88192-6_8.
61. Shrinkage, R. Regression Shrinkage and Selection via the Lasso Author (s): Robert Tibshirani Source : Journal of the Royal Statistical Society . Series B (Methodological), Vol . 58 , No . 1 (1996), Published by : Wiley for the Royal Statistical Society Stable URL. **2016**, 58, 267–288.
62. Velichko, A. Neural Network for Low-Memory IoT Devices and MNIST Image Recognition Using Kernels Based on Logistic Map. *Electron.* **2020**, 9, 1–16, doi:10.3390/electronics9091432.
63. Velichko, A. A Method for Medical Data Analysis Using the Lognnet for Clinical Decision Support Systems and Edge Computing in Healthcare. *Sensors* **2021**, 21, doi:10.3390/s21186209.
64. Velichko, A.; Heidari, H. A Method for Estimating the Entropy of Time Series Using Artificial Neural Networks. *Entropy* **2021**, 23, doi:10.3390/e23111432.
65. Izotov, Y.A.; Velichko, A.A.; Boriskov, P.P. Method for Fast Classification of MNIST Digits on Arduino UNO Board Using LogNNNet and Linear Congruential Generator. *J. Phys. Conf. Ser.* **2021**, 2094, 32055, doi:10.1088/1742-6596/2094/3/032055.
66. Boslaugh, S. *Statistics in a Nutshell, 2nd Edition*; O'Reilly Media, Incorporated, 2012; ISBN 9781449361129.
67. Pandas 1.4.3 Documentation Available online: <https://pandas.pydata.org/docs/reference/api/pandas.DataFrame.corr.html>.
68. Harrington, P. *Machine Learning in Action*; Simon and Schuster, 2012; ISBN 978-1617290183.
69. Feurer, M.; Eggensperger, K.; Falkner, S.; Lindauer, M.; Hutter, F. Auto-Sklearn 2.0: Hands-Free AutoML via Meta-Learning. **2020**.
70. Weiss, G.; Ganz, T.; Goodnough, L.T. Anemia of Inflammation. *Blood* **2019**, 133, 40–50, doi:10.1182/blood-2018-06-856500.
71. Zhang, J. jin; Cao, Y. yuan; Tan, G.; Dong, X.; Wang, B. chen; Lin, J.; Yan, Y. qin; Liu, G. hui; Akdis, M.; Akdis, C.A.; et al. Clinical, Radiological, and Laboratory Characteristics and Risk Factors for Severity and Mortality of 289 Hospitalized COVID-19 Patients. *Allergy Eur. J. Allergy Clin. Immunol.* **2021**, 76, 533–550, doi:10.1111/all.14496.
72. Kim, S.; Kim, D.-M.; Lee, B. Insufficient Sensitivity of RNA Dependent RNA Polymerase Gene of SARS-CoV-2 Viral Genome as Confirmatory Test Using Korean COVID-19 Cases. *Preprints* **2020**, 1–4, doi:10.20944/preprints202002.0424.v1.
73. Teymouri, M.; Mollazadeh, S.; Mortazavi, H.; Naderi Ghale-noie, Z.; Keyvani, V.; Aghababaei, F.; Hamblin, M.R.; Abbaszadeh-Goudarzi, G.; Pourghadamyari, H.; Hashemian, S.M.R.; et al. Recent Advances and Challenges of RT-PCR Tests for the Diagnosis of COVID-19. *Pathol. Res. Pract.* **2021**, 221, 153443, doi:10.1016/j.prp.2021.153443.
74. Djakpo, D.K.; Wang, Z.; Zhang, R.; Chen, X.; Chen, P.; Ketisha Antoine, M.M.L. Blood Routine Test in Mild and Common 2019 Coronavirus (COVID-19) Patients. *Biosci. Rep.* **2020**, 40, 1–5, doi:10.1042/BSR20200817.
75. Fang, B.; Meng, Q.H. The Laboratory's Role in Combating COVID-19. *Crit. Rev. Clin. Lab. Sci.* **2020**, 57, 400–414, doi:10.1080/10408363.2020.1776675.
76. Bertolini, A.; van de Peppel, I.P.; Bodewes, F.A.J.A.; Moshage, H.; Fantin, A.; Farinati, F.; Fiorotto, R.; Jonker, J.W.; Strazza-bosco, M.; Verkade, H.J.; et al. Abnormal Liver Function Tests in Patients With COVID-19: Relevance and Potential Pathogenesis. *Hepatology* **2020**, 72, 1864–1872, doi:10.1002/hep.31480.
77. Terpos, E.; Ntanasis-Stathopoulos, I.; Elalamy, I.; Kastiritis, E.; Sergeantanis, T.N.; Politou, M.; Psaltopoulou, T.; Gerotziafas, G.; Dimopoulos, M.A. Hematological Findings and Complications of COVID-19. *Am. J. Hematol.* **2020**, 95, 834–847, doi:10.1002/ajh.25829.

78. Mao, J.; Dai, R.; Du, R.C.; Zhu, Y.; Shui, L.P.; Luo, X.H. Hematologic Changes Predict Clinical Outcome in Recovered Patients with COVID-19. *Ann. Hematol.* **2021**, *100*, 675–689, doi:10.1007/s00277-021-04426-x.
79. Kočar, E.; Režen, T.; Rozman, D. Cholesterol, Lipoproteins, and COVID-19: Basic Concepts and Clinical Applications. *Biochim. Biophys. Acta - Mol. Cell Biol. Lipids* **2021**, *1866*, doi:10.1016/j.bbalip.2020.158849.
80. Zinellu, A.; Paliogiannis, P.; Fois, A.G.; Solidoro, P.; Carru, C.; Mangoni, A.A. Cholesterol and Triglyceride Concentrations, COVID-19 Severity, and Mortality: A Systematic Review and Meta-Analysis With Meta-Regression. *Front. Public Heal.* **2021**, *9*, 1–14, doi:10.3389/fpubh.2021.705916.
81. Wei, X.; Zeng, W.; Su, J.; Wan, H.; Yu, X.; Cao, X.; Tan, W.; Wang, H. Hypolipidemia Is Associated with the Severity of COVID-19. *J. Clin. Lipidol.* **2020**, *14*, 297–304, doi:10.1016/j.jacl.2020.04.008.
82. Stephens, J.R.; Wong, J.L.C.; Broomhead, R.; Mpfle, R.S.; Waheed, U.; Patel, P.; Brett, S.J.; Soni, S. Raised Serum Amylase in Patients with COVID-19 May Not Be Associated with Pancreatitis. *Br. J. Surg.* **2021**, *108*, 1–2, doi:10.1093/BJS/ZNAA168.
83. Wu, M.Y.; Yao, L.; Wang, Y.; Zhu, X.Y.; Wang, X.F.; Tang, P.J.; Chen, C. Clinical Evaluation of Potential Usefulness of Serum Lactate Dehydrogenase (LDH) in 2019 Novel Coronavirus (COVID-19) Pneumonia. *Respir. Res.* **2020**, *21*, 1–6, doi:10.1186/s12931-020-01427-8.
84. Hu, F.; Guo, Y.; Lin, J.; Zeng, Y.; Wang, J.; Li, M.; Cong, L. Association of Serum Uric Acid Levels with COVID-19 Severity. *BMC Endocr. Disord.* **2021**, *21*, 1–12, doi:10.1186/s12902-021-00745-2.
85. Zinellu, A.; Sotgia, S.; Fois, A.G.; Mangoni, A.A. Serum CK-MB, COVID-19 Severity and Mortality: An Updated Systematic Review and Meta-Analysis with Meta-Regression. *Adv. Med. Sci.* **2021**, *66*, 304–314, doi:10.1016/j.advms.2021.07.001.
86. Afra, H.S.; Amiri-Dashatan, N.; Ghorbani, F.; Maleki, I.; Mostafa-Rezaei-Tavirani Positive Association between Severity of COVID-19 Infection and Liver Damage: A Systematic Review and Meta-Analysis. *Gastroenterol. Hepatol. from Bed to Bench* **2020**, *13*, 292–304, doi:10.22037/ghfbb.v13i4.2129.
87. Huang, Y.; Yang, R.; Xu, Y.; Gong, P. Clinical Characteristics of 36 Non-Survivors with COVID-19 in Wuhan, China. **2020**, doi:10.1101/2020.02.27.20029009.
88. Amin, S.U.; Hossain, M.S. Edge Intelligence and Internet of Things in Healthcare: A Survey. *IEEE Access* **2021**, *9*, 45–59, doi:10.1109/ACCESS.2020.3045115.
89. Vetter, B.; Sampath, R.; Carmona, S. *Landscape of Point-of-Care Devices for Testing of Cardiometabolic Diseases*; 2020;